THE ASTROPHYSICAL JOURNAL, 524:454–461, 1999 October 10

THE MgH $B'\ ^2\Sigma^+$–$X\ ^2\Sigma^+$ TRANSITION: A NEW TOOL FOR STUDYING MAGNESIUM ISOTOPE ABUNDANCES

LLOYD WALLACE AND KENNETH HINKLE
Kitt Peak National Observatory, National Optical Astronomy Observatories,[1] Tucson, AZ 85726; wallace@noao.edu
AND
GANG LI AND PETER BERNATH[2]
Department of Chemistry, University of Waterloo, Waterloo N2L 3G1, Ontario, Canada
Received 1999 January 5; accepted 1999 May 19

ABSTRACT

We have identified lines from the 0–3, 0–4, 0–5, 0–6, 0–7, 1–3, 1–4, 1–7, and 1–8 bands of the ^{24}MgH $B'\ ^2\Sigma^+$–$X\ ^2\Sigma^+$ transition in sunspot umbral spectra. Lines of the 0–7 and 1–8 bands in the uncluttered 7500 Å region are the most obvious, but $B'\ ^2\Sigma^+$–$X\ ^2\Sigma^+$ lines have been tracked as far to the blue as 5300 Å. In combination with weak lines of the 0–7 bands of the ^{25}MgH and ^{26}MgH isotopes, the solar isotope ratio ^{24}Mg:^{25}Mg:^{26}Mg has been measured as 76:12:12, in agreement with the much better determined terrestrial ratio 79:10:11. The intensity distribution of bands with v'' from 4 to 8 has been measured and found to show no anomalies; the excitation temperature of 3100 K agrees well with a value of 3200 K determined from SiO in a sunspot spectrum. The lines of the MgH $B'\ ^2\Sigma^+$–$X\ ^2\Sigma^+$ transition are much more cleanly separated and much less blended than lines from the stronger $A\ ^2\Pi$–$X\ ^2\Sigma^+$ transition. The $B'\ ^2\Sigma^+$–$X\ ^2\Sigma^+$ lines should prove useful in isotopic abundance analyses for stars where the $A\ ^2\Pi$–$X\ ^2\Sigma^+$ transition is too strong to yield useful results.

Subject headings: molecular data — Sun: abundances — sunspots

1. INTRODUCTION

The MgH molecule is of considerable astrophysical interest. The green $A\ ^2\Pi$–$X\ ^2\Sigma^+$ bands are detectable in stellar spectra over a large range of temperatures and abundances (Cottrell 1978). The combination of MgH and Mg I lines has been shown to be a spectroscopic probe of surface gravity in late-type stars (Bonnell & Bell 1993). MgH can also be used to probe the isotopic abundance of magnesium. Magnesium has three stable isotopes, ^{24}Mg, ^{25}Mg, and ^{26}Mg, with terrestrial abundances 78.99:10.00:11.01 (Catanzaro et al. 1966). As reviewed by Tomkin & Lambert (1980), in massive stars, ^{25}Mg and ^{26}Mg are produced during He burning that includes thermal pulsing. ^{24}Mg is produced during carbon burning. Explosive carbon burning can produce all three Mg isotopes. Tomkin & Lambert note that a common feature of these sources of Mg is that the production of ^{25}Mg and ^{26}Mg depends on the initial abundance of heavy elements, but the production of ^{24}Mg is nearly independent of the initial abundance of heavy elements. Thus the current ratio of ^{24}Mg relative to ^{25}Mg and ^{26}Mg is a result of the historic heavy-element abundances, and magnesium isotopes can be used to probe the heavy-element enrichment of the universe. This has been recognized and exploited for some time in the analysis of magnesium isotopic ratios in presolar meteoritic chondrules (e.g., Choi et al. 1998).

Molecular spectra are useful tools for isotopic analysis because the isotopic splitting is frequently larger than the line width. MgH would appear to be an excellent tool to probe the magnesium isotopic ratio. However, astronomical spectroscopy of the pure rotational and vibration-rotation spectrum of magnesium hydride, which would yield spectra with very large separations between the isotopic features, has not been fruitful. The lowest lying MgH rotational frequencies are spin doublets divided into three hyperfine transitions because of the proton nuclear spin (Ziurys, Barclay, & Anderson 1993; Zink et al. 1990). The lines are found in the submillimeter region and have been searched for in circumstellar shells but so far have not been detected (Avery et al. 1994). The vibration-rotation fundamental is at 6.7 μm (Bernath, Black, & Brault 1985; Lemoine et al. 1988), a spectral region not accessible to ground-based observers.

The well-known visible region electronic $A\ ^2\Pi$–$X\ ^2\Sigma^+$ bands are in an easily studied part of the spectrum near 5200 Å (Balfour 1970; Bernath et al. 1985). While our knowledge of the Mg isotopic ratio in stars depends on the $A\ ^2\Pi$–$X\ ^2\Sigma^+$ transition (e.g., Shetrone 1996; McWilliam & Lambert 1988; Barbuy, Spite, & Spite 1987; Barbuy 1985, 1987; Lambert & McWilliam 1986; Tomkin & Lambert 1976,1980), this is a difficult observational problem because the isotopic splitting of the MgH A–X lines is small, typically 0.1 Å for the (0, 0) band. High resolution, high signal-to-noise ratio (S/N), and spectrum synthesis are required in order to measure the isotopic ratio. Isotopic splitting for the weaker (0, 1) and (1, 2) bands is larger (0.4 Å), but the spectrum is complex with many blends. In addition, the TiO α-system contaminates the region of the (0, 1) and (1, 2) bands.

While preparing an atlas of a sunspot umbral spectrum, we identified three series of regularly spaced lines with large interline spacing indicative of a hydride (Wallace et al. 1998). We were later able to identify these lines as due to the 0–7 and 1–8 bands of the $B'\ ^2\Sigma^+$–$X\ ^2\Sigma^+$ transition of ^{24}MgH and extend the identifications to include the 0–6, 0–5, 0–4, 0–3, 1–7, 1–4, and 1–3 bands. Extensive laboratory work on this transition in MgH has previously been under-

[1] Operated by the Association of Universities for Research in Astronomy, Inc. under cooperative agreement with the National Science Foundation.
[2] Also, Department of Chemistry, University of Arizona, Tucson, AZ 85721.

TABLE 1

OBSERVED LINES OF THE B'–X TRANSITION OF ^{24}MgH IN THE SUNSPOT SPECTRUM[a]

Wavenumber (cm^{-1})	Line	EW (mK)
0–7 Band		
13193.61	*P*(15)	31.2
13205.15w	*R*(19)	29.3
13237.05	*P*(14)	37.6
13242.93w	*R*(18)	35.0
13278.84	*P*(13)	39.6
13280.11w	*R*(17)	30.7
13316.39	*R*(16)	...
13318.80	*P*(12)	...
13351.47	*R*(15)	30.9
13356.71	*P*(11)	30.5
13385.11	*R*(14)	46.6
13392.43	*P*(10)	33.6
13416.97	*R*(13)	32.3
13425.78	*P*(9)	24.7
13446.96	*R*(12)	45.7
13456.70	*P*(8)	26.6
13474.86	*R*(11)	35.2
13485.04	*P*(7)	21.3
13500.49	*R*(10)	36.2
13510.67	*P*(6)	...
13523.74	*R*(9)	27.0
13533.51	*P*(5)	...
13544.47	*R*(8)	28.5
13562.57	*R*(7)	24.6
13577.93	*R*(6)	22.1
13584.94	*P*(2)	...
13600.26	*R*(4)	...
13607.03	*R*(3)	...
13610.87	*R*(2)	...
0–6 Band		
13190.60d	*P*(28)	43.9
13256.76d	*P*(27)	59.2
13324.83d	*P*(26)	51.3
13363.38d	*R*(30)	39.8
13394.04d	*P*(25)	63.1
13413.75d	*R*(29)	45.2
13463.80w	*P*(24)	54.3
13468.44d	*R*(28)	...
13738.70	*P*(20)	...
13804.61	*P*(19)	51.9
14108.39	*R*(17)	56.1
14156.84	*P*(13)	...
14158.82	*R*(16)	55.5
14206.61	*P*(12)	54.8
14206.85	*R*(15)	54.8
14297.17	*P*(10)	34.1
14337.75	*P*(9)	...
14405.25	*R*(10)	...
14435.66	*R*(9)	...
14439.50	*P*(6)	25.8
14526.15	*P*(2)	...
1–8 Band		
13346.85	*P*(14)	39.8
13372.71	*P*(13)	24.0
13398.60	*P*(12)	...
13423.95	*P*(11)	...
13448.42	*P*(10)	31.2
13471.80	*P*(9)	26.2
13493.88	*P*(8)	17.8

TABLE 1—*Continued*

Wavenumber (cm^{-1})	Line	EW (mK)
13494.45	*R*(14)	...
13514.50	*P*(7)	27.4
13527.31	*R*(12)	29.2
13542.34	*R*(11)	33.7
13550.76	*P*(5)	14.7
13569.96	*R*(9)	...
13581.87	*R*(8)	21.2
13592.23	*R*(7)	...
13607.90	*R*(5)	...
0–5 Band		
13508.06d	*P*(33)	...
13595.72d	*P*(32)	...
13685.70d	*P*(31)	...
13777.18d	*P*(30)	...
14237.01	*P*(25)	...
14239.89w	*R*(28)	76.3
14414.50	*P*(23)	...
14584.70	*P*(21)	81.8
14666.55	*P*(20)	...
14725.08	*R*(22)	...
14745.82	*P*(19)	84.0
14822.42	*P*(18)	94.6
14896.23	*P*(17)	...
14942.21	*R*(19)	...
14967.00	*P*(16)	...
15009.35	*R*(18)	59.6
15034.68	*P*(15)	...
15073.52	*R*(17)	71.7
15099.05	*P*(14)	86.9
15134.66	*R*(16)	67.2
15160.02	*P*(13)	69.2
15192.54	*R*(15)	...
15217.47	*P*(12)	68.1
15247.07	*R*(14)	...
15298.15	*R*(13)	83.5
15321.39	*P*(10)	59.0
15389.47	*R*(11)	...
15410.12	*P*(8)	...
15429.45	*R*(10)	...
15448.59	*P*(7)	...
15465.61	*R*(9)	...
15483.00	*P*(6)	51.2
15497.85	*R*(8)	...
15570.34	*R*(5)	...
15586.26	*R*(4)	...
1–7 Band		
14124.76	*P*(12)	...
14162.53	*P*(11)	...
14191.01d?	*R*(14)	...
14198.15	*P*(10)	...
14280.92	*R*(11)	...
0–4 Band		
14957.45	*R*(30)	...
15062.38	*R*(29)	69.5
15107.35	*P*(26)	62.5
15165.97	*R*(28)	...
15213.99	*P*(25)	...
15267.86	*R*(27)	...
15318.38	*P*(24)	65.5
15465.61	*R*(25)	...
15519.37	*P*(22)	67.9

TABLE 1—*Continued*

Wavenumber (cm^{-1})	Line	EW (mK)
15561.01	*R*(24)	...
15615.65	*P*(21)	...
15708.90	*P*(20)	...
15743.80	*R*(22)	...
15830.84	*R*(21)	...
15885.62	*P*(18)	...
16264.10	*P*(13)	55.3
16282.03	*R*(15)	...
16344.15	*R*(14)	...
16387.72	*P*(11)	...
16402.22	*R*(13)	...
16443.22	*P*(10)	...
16456.16	*R*(12)	...
16494.39	*P*(9)	...
16505.78	*R*(11)	...
16541.06	*P*(8)	...
16551.19	*R*(10)	...
1–4 Band		
16269.70w	*R*(25)	...
16325.20	*P*(22)	...
16366.09	*R*(24)	...
16458.93	*R*(23)	...
16514.96	*P*(20)	...
16549.22	*R*(22)	...
16605.04	*P*(19)	...
16636.50	*R*(21)	...
16691.68	*P*(18)	...
16720.58	*R*(20)	...
16774.87	*P*(17)	...
16801.32	*R*(19)	...
16854.32	*P*(16)	...
16878.57	*R*(18)	...
17002.58	*P*(14)	...
17070.15	*P*(13)	...
17133.95	*P*(12)	...
17150.10	*R*(14)	...
17193.56	*P*(11)	...
17248.93	*P*(10)	...
17299.97	*P*(9)	...
17311.93	*R*(11)	...
17346.63	*P*(8)	...
17357.26	*R*(10)	...
17388.84	*P*(7)	...
17398.15	*R*(9)	...
17426.59	*P*(6)	...
17494.03	*R*(6)	...
17516.87	*R*(5)	...
1–3 Band		
16341.26	*P*(31)	...
16473.62	*P*(30)	...
16517.06	*R*(32)	...
16603.90	*P*(29)	...
16642.44	*R*(31)	...
16731.92	*P*(28)	...
16766.68	*R*(30)	...
16857.35	*P*(27)	...
16888.77	*R*(29)	...
17100.35	*P*(25)	...
17217.19	*P*(24)	...
17239.72	*R*(26)	...
17330.87	*P*(23)	...
17441.15	*P*(22)	...
17459.51	*R*(24)	...

TABLE 1—*Continued*

Wavenumber (cm^{-1})	Line	EW (mK)
17547.92	*P*(21)	...
17563.93	*R*(23)	...
17651.02	*P*(20)	...
17750.31	*P*(19)	...
17762.78	*R*(21)	...
17845.65	*P*(18)	...
17936.95	*P*(17)	...
17946.66	*R*(19)	...
18114.28	*R*(17)	...
18329.33	*P*(12)	...
18454.34	*P*(10)	...
18509.52	*P*(9)	...
18512.55	*R*(11)	...
18605.96	*P*(7)	...
0–3 Band		
16635.32	*P*(22)	...
16758.79	*R*(23)	...
17050.78	*R*(20)	...
17130.89	*P*(17)	...
17218.08	*P*(16)	...
17308.15	*R*(17)	...
17458.90	*R*(15)	...
17523.37	*P*(12)	...
17651.53	*R*(12)	...

[a] The unit mK is 10^{-3} cm^{-1}. The letter d or w after an observed wavenumber indicates a line that is double or wider than the lower N lines, respectively.

taken by Balfour & Cartwright (1976) and Balfour & Lindgren (1978). In contrast to the $A\ ^2\Pi$ and $X\ ^2\Sigma^+$ states, the $B'\ ^2\Sigma^+$ and $X\ ^2\Sigma^+$ states have very different potential curves, with the result that the 0–0 band is very weak and the spectrum is dominated by vibrational transitions of exceptionally large Δv. To our knowledge there has been no previous detection of the $B'\ ^2\Sigma^+$–$X\ ^2\Sigma^+$ system of MgH either in astronomical sources or in absorption in the laboratory.

Measurements of the frequencies of the ^{24}MgH B'–X lines in the sunspot umbral spectrum are presented, along with equivalent widths. A few weak lines due to ^{25}MgH and ^{26}MgH show that the large isotopic shifts in this transition can be used to allow a very straightforward extraction of the isotopic ratio. Spectroscopic constants are derived from the observed laboratory and sunspot frequencies, which allow calculation of a full set of line frequencies. We also present Franck-Condon factors and line-strength factors, which include the variation due to the dipole moment function and the rotational energy, and use them to examine the population distribution.

2. LABORATORY SPECTROSCOPY OF MgH

Laboratory spectroscopy of MgH, driven by the need to identify strong bands seen in astronomical spectra, dates back to at least 1909 (King 1916 and references therein). Analyses of the well-known $A\ ^2\Pi$–$X\ ^2\Sigma^+$ system of MgH were reported, for example, by Balfour (1970) and by Bernath et al. (1985).

Balfour & Cartwright (1976) and Balfour & Lindgren (1978) reported on the analysis of the emission spectra of the $B'\ ^2\Sigma^+$–$X\ ^2\Sigma^+$ transition of ^{24}MgH, ^{25}MgH, ^{26}MgH,

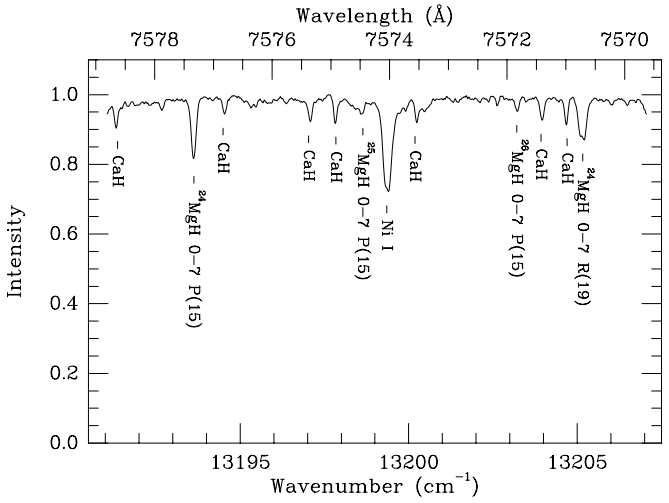

FIG. 1.—Section of the sunspot umbral spectrum, 1981/03/24 No. 1, showing four lines of the 0–7 band of the $B'–X$ transition of various isotopes of MgH, as well as CaH and a Ni I line. The CaH wavenumbers used for positioning the identifying labels were determined from laboratory studies and show small mismatches with the features in the umbral spectrum.

^{24}MgD, ^{25}MgD, and ^{26}MgD, thereby establishing beyond any doubt the vibrational numbering and the nature of the B' state. The potential energy curve of the B' state is displaced to appreciably larger radial distance than that of the X state, with the result that the strongest bands are not the usual ones described by a narrow diagonal parabola in the (v', v'')-plane emphasizing the $\Delta v = 0$ sequence, but rather the strongest bands are on a broad Condon parabola such that bands with low v' and $v'' \sim 3$–8 are relatively strong and appear at wavenumbers that are much less than the system origin at 22082 cm^{-1}, as well as those with low v'' and $v' \sim 3$–8, which appear at wavenumbers that are much more than the system origin. The bands are headless and strongly degraded to the red.

Balfour & Lindgren (1978) calculated approximate rotationless Franck-Condon factors for the range $v' = 0$–3 and $v'' = 4$–9, which includes the bands we have observed. Kirby, Saxon, & Liu (1979) present rotationless band oscillator strengths including the dipole moment function of Saxon, Kirby, & Liu (1978) for the range $v' = 0$–14 and $v'' = 0$–3, which excludes most of the bands we have observed. Sink & Bandrauk (1979) have also calculated rotationless Franck-Condon factors and band strengths for $v' = 0$–6 and $v'' = 0$–8.

TABLE 2

OBSERVED LINES OF THE $B'–X$ 0–7 BAND OF ^{25}MgH AND ^{26}MgH IN THE SUNSPOT SPECTRUM[a]

Wavenumber (cm^{-1})	Line	EW (mK)
^{25}MgH		
13198.60.....	$P(15)$	5.04
13356.20.....	$R(15)$	6.33
13421.79.....	$R(13)$	4.36
^{26}MgH		
13203.21.....	$P(15)$	7.42
13288.54.....	$P(13)$	5.16
13328.52.....	$P(12)$	4.95

[a] The unit mK is 10^{-3} cm^{-1}.

3. OBSERVATIONS AND MEASUREMENTS

The primary sunspot umbral spectrum used was obtained by L. Testerman with the Brault 1 m Fourier transform spectrometer (FTS) at the McMath-Pierce telescope on Kitt Peak. The spectrum, which is in the archives of the National Solar Observatory,[3] is identified by date and number as 1981/03/24 No. 1. This spectrum has good S/N from 9000 to 16500 cm^{-1} and includes most of the bands of interest here. Beyond 16500 cm^{-1}, we have used another FTS spectrum obtained by Testerman, 1981/03/25 No. 1, which extends to 23000 cm^{-1}.

Wallace et al. (1998) reported three unidentified branches consisting of a total of 33 lines in the relatively uncluttered spectral region between 13173 and 13580 cm^{-1}. This region is bounded at short wavenumbers by the strong 0–1 head of the TiO γ bands (Ram et al. 1999) and at long wavenumbers by the increasing strength of lines of the red-degraded bands of the $\Delta v = -1$ sequence of the CaH $A–X$ bands and the $\Delta v = 0$ sequence of the TiO γ bands. We have recently identified the branches on the basis of ^{24}MgH $B'–X$ line positions calculated from the term values given by Balfour & Cartwright and Balfour & Lindgren. Two of the three branches are the P and R branches of the 0–7 band, and the third is the P branch of the 1–8 band. We have also found lines of the 0–6, 0–5, 0–4, 0–3, 1–7, 1–4, and 1–3 bands. We could not find any lines from bands with $v' = 2$. Bands with $v'' = 0$ and 1 on the leg of the Condon parabola opposite to the $v' = 0$ and 1 progressions observed here (Kirby et al. 1979) should have similar strengths, but they fall at frequencies larger than 23000 cm^{-1}, outside of the range covered by our spectra.

Our measurements of the ^{24}MgH line positions in the sunspot umbral spectra, taken in part from Wallace et al., and the vibrational and rotational assignments, made with the help of the term values of Balfour & Cartwright and Balfour & Lindgren, are given in Table 1. We have subsequently obtained lists of the observed laboratory wavenumbers of the lines that were used in the analyses from W. J. Balfour. (These are the unpublished Tables 1, 2, and 3 of Balfour & Lindgren.) We have calibrated the line positions of the two sunspot spectra from Ti I lines common to both the sunspot and the laboratory spectra of Ti I, also obtained with the Brault 1 m FTS, and reported by Forsberg (1991). The laboratory and sunspot $B'–X$ line positions generally agree to better than 0.05 cm^{-1}, the estimated accuracy of the laboratory data. The strong lines in the sunspot spectrum have an absolute accuracy of about 0.02 cm^{-1}.

A small piece of the umbral spectrum, given as Figure 1, illustrates the appearance of the P and R lines of ^{24}MgH, as well as the weak lines of ^{25}MgH and ^{26}MgH. The isotopic shifts are large, ~ 5 cm^{-1} for ^{25}MgH and ~ 10 cm^{-1} for ^{26}MgH. Generally, the P and R lines of ^{24}MgH appear sharp at low rotational quantum number N, become slightly broader as N increases, and at large enough N become double. This is due to the small spin-splitting reported by Balfour & Lindgren. The lines of ^{25}MgH and ^{26}MgH that have been identified from the frequency lists of W. J. Balfour are weak and frequently blended with other features, as indicated in Figure 1.

[3] See http://www.nso.noao.edu/, which is maintained at NOAO.

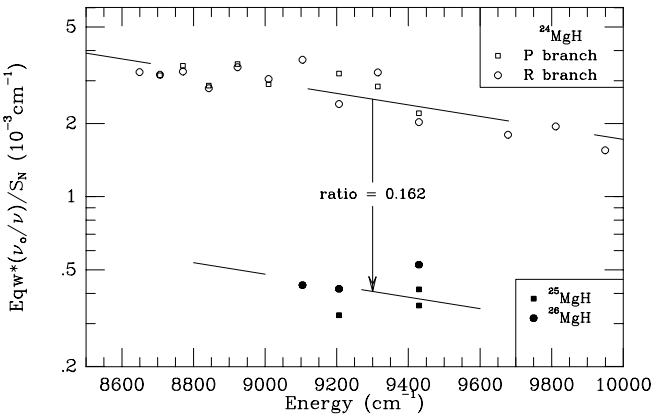

FIG. 2.—Equivalent widths of lines of the 0–7 band of the B'–X transition of ^{24}MgH, ^{25}MgH, and ^{26}MgH, scaled by frequency (ν) and the Hönl-London factor (S_N) and plotted against ground-state energy.

We have measured equivalent widths of the ^{24}MgH lines that appear relatively clean and are not substantially confused with other features. These measurements are added to Table 1. We have also measured as many ^{25}MgH and ^{26}MgH lines as seem reasonably clear, but there are very few. The ^{25}MgH $P(15)$ line at 13198.6 cm^{-1}, illustrated in Figure 1, is clearly blended, whereas the ^{26}MgH $P(15)$ line at 13203.2 cm^{-1}, also included in Figure 1, appears relatively clean. The results for the few good lines are given in Table 2.

4. MAGNESIUM ISOTOPIC ABUNDANCE

Since the only clean lines of the heavy isotopes are from the 0–7 band, it suffices to intercompare only lines of the 0–7 band of all three isotopes. Also, since the MgH B'–X lines are essentially fully resolved and truly shallow, we have treated them as unsaturated and, therefore, interpreted the equivalent widths as

$$\mathrm{EW} = \text{constant}\,(\text{isotope})(\nu/\nu_0)S_N e^{-Ehc/kT}, \qquad (1)$$

where *constant* is a constant depending on isotope amount, ν and ν_0 are line and reference frequencies, S_N is the Hönl-London factor, E is the lower state energy, T is an excitation temperature, and hc/k is the second radiation constant. The resulting values are shown on the standard plot in Figure 2, where a linear least-squares fit to the ^{24}MgH data is indicated. The slope of the fit, applied to the totality of the ^{25}MgH and ^{26}MgH material, yields the indicated ratio of 0.162 and the isotopic ratio ^{24}Mg:^{25}Mg:^{26}Mg = 76:12:12 with a 1 σ uncertainty of 3 in each factor. The use of the rotationless Hönl-London factors here is not a source of error, because lines of the same transition, for the most part, are being compared.

5. SPECTROSCOPIC CONSTANTS

To provide a simple scheme for obtaining good line positions for the full set of lines, we have combined our sunspot measurements reported in Table 1 with the previously measured lines of Balfour & Lindgren (1978). In this fit, only the bands with $v' = 0$ and 1 are included and the lower state vibrational levels range from 3 to 9 for ^{24}MgH. The spin splitting was not usually resolved, so the simple energy level expression

$$E_v(N) = T_v + B_v N(N+1) - D_v[N(N+1)]^2 + H_v[N(N+1)]^3 + L_v[N(N+1)]^4 \qquad (2)$$

was used. The vibrational term value $T_{v=3}$ was set to zero in these fits (Table 3). Perturbed lines were included but with lower weights. A more comprehensive fit including additional bands as well as the infrared and pure rotational data will be published separately.

Similar fits, but using only the measurements of Balfour & Lindgren, were carried out for ^{25}MgH and ^{26}MgH. The constants from these fits are also included in Tables 3 and 4. The spectroscopic data for these minor isotopomers are much less extensive than for ^{24}MgH.

6. POPULATION DISTRIBUTION

We have looked into the question of why these bands are observed in absorption at all. Balfour & Cartwright (1975) were not able to find them in absorption in the laboratory, and Tomkin & Lambert (1980) could not find them in stellar spectra.

To pursue this question, we have calculated relative band strengths. Rydberg-Klein-Rees (RKR) potentials for the B' and X states were generated from the constants B_v and T_v of Tables 3 and 4 plus those for $v'' = 0$–2 from Lemoine et al. (1988). Franck-Condon factors were calculated and found to be in general agreement with the rotationless values of Balfour & Cartwright (1976). However, for a light metal hydride such as MgH with shallow electronic states, the Franck-Condon factors are expected to be N-dependent. This was found to be the case, and the values computed for $N = 0, 5, \ldots, 30$ are reported in Table 5. In addition, the transition dipole moment has a strong variation with radial distance R, so the line-strength factors $[M^{v',N'}_{v'',N''}]^2$ were computed using the ab initio dipole moment function μ of Saxon et al. (1978). The line-strength factors are given by

$$[M^{v',N'}_{v'',N''}]^2 = \langle v'N' \,|\, \mu \,|\, v''N'' \rangle^2 \qquad (3)$$

(Bernath 1995). (With the dipole moment operator μ set to unity and N' and N'' set to zero, this expression gives the

TABLE 3

SPECTROSCOPIC CONSTANTS FOR THE B' STATE OF MgH[a]

	^{24}MgH		^{25}MgH		^{26}MgH	
PARAMETER	$v = 0$	$v = 1$	$v = 0$	$v = 1$	$v = 0$	$v = 1$
T_v	17980.132(13)	18785.272(12)	17983.222(42)	18787.716(44)	17986.187(40)	18790.115(42)
B_v	2.596143(103)	2.603246(110)	2.592650(258)	2.600418(305)	2.587923(269)	2.594949(309)
$D_v \times 10^4$	1.05994(179)	1.18479(193)	1.08068(524)	1.22824(727)	1.04758(549)	1.16777(727)
$H_v \times 10^9$	6.655(89)	7.334(94)	8.485(305)	11.458(543)	6.092(330)	6.507(515)

[a] Units throughout are cm^{-1}. In this table, the numbers in parentheses are 1 σ uncertainties in the last quoted figure.

TABLE 4

SPECTROSCOPIC CONSTANTS FOR THE X STATE OF MgH[a]

PARAMETER	$v = 3$	$v = 4$	$v = 5$	$v = 6$	$v = 7$	$v = 8$	$v = 9$
			^{24}MgH				
T_v	0.0[b,c]	1229.151(14)	2377.404(15)	3432.512(17)	4375.755(15)	5177.379(20)	5790.490(27)
B_v	5.171278(150)	4.956808(150)	4.720139(167)	4.446440(228)	4.108027(239)	3.663275(642)	3.01210(139)
$D_v \times 10^4$.....	3.74393(346)	3.87391(459)	4.19669(680)	4.8469(117)	5.8805(183)	8.4946(737)	14.209(157)
$H_v \times 10^9$	15.116(325)	7.035(600)	3.99(112)	17.19(231)	5.67(524)	217.6(308)	0.0[b]
$L_v \times 10^{11}$.....	−0.8015(109)	−1.2512(269)	−2.9093(597)	−8.774(147)	−24.112(475)	−124.50(418)	0.0[b]
			^{25}MgH				
T_v	0.0[b]	1228.255(44)	2375.859(46)	3430.792(50)	4374.298(53)	5176.417(80)	...
B_v	5.161736(486)	4.949907(311)	4.715195(388)	4.435461(509)	4.092435(564)	3.64193(160)	...
$D_v \times 10^4$.....	3.6577(119)	3.8547(100)	4.2530(131)	4.3858(174)	4.9672(229)	6.251(106)	...
$H_v \times 10^9$	2.20(88)	2.63(143)	14.48(180)	−95.56(169)	−248.04(283)	−689.8(208)	...
$L_v \times 10^{11}$.....	0.0[b]	−0.8625(725)	−3.360(86)	0.0[b]	0.0[b]	0.0[b]	...
			^{26}MgH				
T_v	0.0[b]	1227.609(41)	2374.672(43)	3429.039(46)	4372.162(62)	5174.307(93)	...
B_v	5.153138(449)	4.940446(285)	4.707348(379)	4.435695(580)	4.10122(109)	3.67095(298)	...
$D_v \times 10^4$.....	3.5950(101)	3.7136(62)	4.1634(128)	4.7947(295)	5.9438(710)	9.977(319)	...
$H_v \times 10^9$	−2.26(68)	−16.15(40)	4.32(182)	11.7(59)	35.0(181)	968.(129)	...
$L_v \times 10^{11}$.....	0.0[b]	0.0[b]	−2.887(90)	−8.082(389)	−25.66(155)	−238.0(176)	...

[a] Units throughout are cm^{-1}. In this table, the numbers in parentheses are 1 σ uncertainties in the last quoted figure.
[b] Fixed.
[c] $T_3 = 4102.35$ cm^{-1}, using the term values of Balfour & Lindgren 1978.

rotationless Franck-Condon factors.) The line strengths were then generated for $N' = N'' = 0, 5, \ldots, 30$ for $v' = 0$ and 1 and $v'' = 0$–8. These factors are reported in Table 6, in atomic units $(ea_0)^2$. Values are missing in Tables 5 and 6 at high N for $v'' = 7$ and 8 because of dissociation. We note that for some bands, the dependence on rotational energy is large. Additionally, the contrast between Tables 5 and 6 shows that the inclusion of the R dependence of the transition dipole moment changes the relative band strengths significantly.

For the single isotope, ^{24}MgH, the inclusion of M^2 in equation (1) gives

$$\mathrm{EW} = \text{constant} \times M^2(\nu/\nu_0)S_N e^{-Ehc/kT} \qquad (4)$$

and suggests the standard plot in Figure 3. Here, the EWs of individual lines of different bands are scaled and plotted against lower state energy. The points for the different bands show scatter apparently due to the difficulty of measurement, but there are no clear separations indicating preferential excitation of the high-v'' levels.

A least-squares fit to the data yields the linear fit in Figure 3, which gives an excitation temperature $T_{ex} = 3110$ K. This is in quite good agreement with the $T_{ex} = 3200$ K determined from SiO in a similarly large spot (Campbell et al. 1995). Thus, there appears to be nothing extraordinary about the population distribution. These bands are, however, much weaker than the A–X bands, as Kirby et al. (1979) have noted.

7. DISCUSSION

Previous determinations of the Mg isotope ratio from the

TABLE 5

FRANCK-CONDON FACTORS FOR THE B'–X TRANSITION OF MgH[a]

		v''								
v'	N	0	1	2	3	4	5	6	7	8
0.....	0	3.15(−5)	5.70(−4)	4.86(−3)	2.54(−2)	8.88(−2)	2.10(−1)	3.22(−1)	2.71(−1)	7.41(−2)
	5	3.19(−5)	5.81(−4)	4.96(−3)	2.60(−2)	9.10(−2)	2.15(−1)	3.26(−1)	2.67(−1)	6.65(−2)
	10	3.31(−5)	6.11(−4)	5.27(−3)	2.78(−2)	9.73(−2)	2.28(−1)	3.35(−1)	2.54(−1)	4.69(−2)
	15	3.57(−5)	6.71(−4)	5.88(−3)	3.13(−2)	1.09(−1)	2.51(−1)	3.50(−1)	2.25(−1)	1.90(−2)
	20	4.05(−5)	7.80(−4)	6.96(−3)	3.73(−2)	1.30(−1)	2.87(−1)	3.62(−1)	1.67(−1)	1.23(−4)
	25	4.94(−5)	9.79(−4)	8.91(−3)	4.81(−2)	1.64(−1)	3.42(−1)	3.53(−1)	6.54(−2)	...
	30	6.66(−5)	1.36(−3)	1.26(−2)	6.79(−2)	2.24(−1)	4.13(−1)	2.60(−1)	...	...
1.....	0	3.07(−4)	4.16(−3)	2.49(−2)	8.26(−2)	1.52(−1)	1.21(−1)	4.05(−3)	1.47(−1)	3.75(−1)
	5	3.09(−4)	4.20(−3)	2.52(−2)	8.36(−2)	1.53(−1)	1.19(−1)	2.68(−3)	1.61(−1)	3.75(−1)
	10	3.14(−4)	4.32(−3)	2.61(−2)	8.65(−2)	1.55(−1)	1.12(−1)	3.05(−4)	2.00(−1)	3.64(−1)
	15	3.27(−4)	4.58(−3)	2.78(−2)	9.17(−2)	1.59(−1)	9.93(−2)	2.20(−3)	2.75(−1)	3.06(−1)
	20	3.54(−4)	5.04(−3)	3.09(−2)	1.00(−1)	1.62(−1)	7.62(−2)	2.45(−2)	3.87(−1)	1.31(−1)
	25	4.05(−4)	5.88(−3)	3.61(−2)	1.13(−1)	1.62(−1)	3.98(−2)	1.12(−1)	4.42(−1)	...
	30	5.01(−4)	7.39(−3)	4.49(−2)	1.32(−1)	1.49(−1)	1.97(−3)	3.52(−1)	...	...

[a] In this table, the number in parentheses following an entry is the power of 10 by which the entry is to be multiplied.

TABLE 6

LINE-STRENGTH FACTORS, M^2, FOR THE B'–X TRANSITION OF MgH[a,b]

		v''								
v'	N	0	1	2	3	4	5	6	7	8
0.....	0	1.27(−5)	2.97(−4)	3.14(−3)	2.00(−2)	8.36(−2)	2.34(−1)	4.17(−1)	4.02(−1)	1.23(−1)
	5	1.31(−5)	3.06(−4)	3.25(−3)	2.07(−2)	8.66(−2)	2.41(−1)	4.25(−1)	3.99(−1)	1.10(−1)
	10	1.43(−5)	3.35(−4)	3.58(−3)	2.28(−2)	9.52(−2)	2.62(−1)	4.47(−1)	3.86(−1)	7.81(−2)
	15	1.65(−5)	3.91(−4)	4.21(−3)	2.69(−2)	1.12(−1)	3.00(−1)	4.81(−1)	3.50(−1)	3.14(−2)
	20	2.05(−5)	4.93(−4)	5.35(−3)	3.43(−2)	1.40(−1)	3.61(−1)	5.19(−1)	2.65(−1)	9.94(−5)
	25	2.80(−5)	6.81(−4)	7.46(−3)	4.77(−2)	1.90(−1)	4.56(−1)	5.29(−1)	1.05(−1)	...
	30	4.27(−5)	1.05(−3)	1.16(−2)	7.36(−2)	2.80(−1)	5.85(−1)	4.02(−1)	...	...
1.....	0	1.06(−4)	1.88(−3)	1.41(−2)	5.73(−2)	1.26(−1)	1.18(−1)	4.19(−3)	1.95(−1)	5.47(−1)
	5	1.08(−4)	1.93(−3)	1.45(−2)	5.86(−2)	1.28(−1)	1.17(−1)	2.74(−3)	2.14(−1)	5.49(−1)
	10	1.16(−4)	2.07(−3)	1.55(−2)	6.25(−2)	1.34(−1)	1.13(−1)	2.53(−4)	2.70(−1)	5.36(−1)
	15	1.30(−4)	2.33(−3)	1.75(−2)	6.96(−2)	1.43(−1)	1.03(−1)	2.95(−3)	3.78(−1)	4.53(−1)
	20	1.55(−4)	2.79(−3)	2.09(−2)	8.12(−2)	1.55(−1)	8.35(−2)	3.15(−2)	5.42(−1)	1.91(−1)
	25	2.00(−4)	3.60(−3)	2.67(−2)	9.92(−2)	1.66(−1)	4.63(−2)	1.48(−1)	6.28(−1)	...
	30	2.82(−4)	5.06(−3)	3.67(−2)	1.27(−1)	1.64(−1)	2.52(−3)	4.78(−1)	...	...

[a] In this table, the number in parentheses following an entry is the power of 10 by which the entry is to be multiplied.
[b] In atomic units $(ea_0)^2$.

very strong MgH A–X transition in sunspot spectra by Kumar (1969), Branch (1970), and Boyer, Henoux, & Sotirovski (1971) have yielded ^{24}Mg:^{25}Mg:^{26}Mg = 64:18:18, 60:20:20, and 80:10:10, respectively, with only the last close to the terrestrial ratio of 79:10:11. These bands in the umbral spectrum are so strong that uncertainties in the continuum placement alone make their interpretation questionable. Lambert, Mallia, & Petford (1971) concluded that this plus other effects produced the apparent overabundance of the heavier isotopes and that umbra and photosphere show isotopic abundances not greater than the terrestrial values.

The solar isotopic magnesium abundance has also been deduced from energetic particle measurements of coronal material. Mewaldt & Stone (1989) give coronal ratios that yield ^{24}Mg:^{25}Mg:^{26}Mg = 75:12:13. Selesnick et al. (1993), using the same technique, suggest a slightly different ratio of 76:12:12. These should match the much-quoted terrestrial "benchmark" ratio of 78.99:10.00:11.01 obtained by Catanzaro et al. (1966) with quoted errors $\pm$0.03:$\pm$0.01:$\pm$0.02.

The 0–7 band of the MgH $B'\ ^2\Sigma^+$–$X\ ^2\Sigma^+$ transition is weak in the umbra and the lines of the isotopes are well separated. This allows a simple, direct analysis that gives ^{24}Mg:^{25}Mg:^{26}Mg = 76:12:12 with an uncertainty of 3 units in each factor. While these uncertainties are comparable to the best solar and coronal determinations, they are an order of magnitude larger than the uncertainties of Catanzaro et al. (1966). Analyses designed to measure the heavy-isotope lines should be able to reduce considerably the uncertainties in a spectroscopic determination by using the $B'\ ^2\Sigma^+$–$X\ ^2\Sigma^+$ lines. In spectra of cool stars where the MgH A–X bands are too strong to be applied to isotopic determinations, the much weaker MgH 0–7 band should prove very useful.

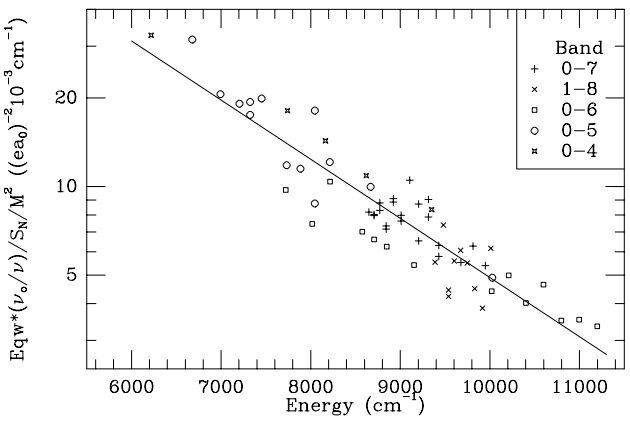

FIG. 3.—Equivalent widths of lines of a number of bands of the B'–X transition of ^{24}MgH scaled as in Fig. 2 and by the line-strength factors (M^2).

A major question is why we have observed the B'–X bands for the first time when attempts to observe them in absorption in the laboratory and in other stellar sources have not been successful (Balfour & Cartwright 1975; Tomkin & Lambert 1980). As noted above, the B'–X bands have a bimodal intensity distribution with the bands near the system origin being undetectable. Our detection is principally of lines in the red. The relative simplicity of the solar spectrum in the red makes detection of weak lines possible. The high density of blending lines in the violet, where we believe others have looked, may well have interfered with the detection of these bands.

The shift between the potential wells of the B' and X states, the high vibrational levels observed, and the umbral origin of our spectra all suggest that non-LTE effects might be preferentially populating the high-v levels of the ground state. In pursuit of this question we have measured the strength of as many of the lines of other bands of this transition as we can find, reaching down to the 0–4 band. Lines of the 0–3 and 1–3 bands were also found, but the overlap with other features prevented reliable equivalent width measurement. We have used the laboratory and sunspot frequencies to determine improved spectroscopic constants. These new constants were used to calculate the RKR potential curves, and with the ab initio transition dipole moment function of Saxon et al. (1978), relative band strengths were obtained. We find the measurements over the range of all the vibrational levels to be consistent and yield an excitation temperature of 3100 K. This is in close agreement with the 3200 K value we obtained from SiO in a similar sunspot.

We conclude that the interpretation of the observed equivalent widths is consistent with LTE processes.

Professor W. J. Balfour kindly provided unpublished wavenumbers for the $B'-X$ lines. We thank Professor R. J. Le Roy for assistance in using his programs to calculate Franck-Condon factors and line strengths. This work was supported in part by the NASA laboratory astrophysics program and the Natural Sciences and Engineering Research Council of Canada. P.B. is grateful for a Killam Research Fellowship.

REFERENCES

Avery, L. W., Bell, M. B., Cunningham, C. T., Feldman, P. A., Hayward, R. H., MacLeod, J. M., Matthews, H. E., & Wade, J. D. 1994, ApJ, 426, 737
Balfour, W. J. 1970, ApJ, 162, 1031
Balfour, W. J., & Cartwright, H. M. 1975, Chem. Phys. Lett., 32, 82
———. 1976, Canadian J. Phys., 54, 1898
Balfour, W. J., & Lindgren, B. 1978, Canadian J. Phys., 56, 767
Barbuy, B. 1985, A&A, 151, 189
———. 1987, A&A, 172, 251
Barbuy, B., Spite, F., & Spite, M. 1987, A&A, 178, 199
Bernath, P. F. 1995, Spectra of Atoms and Molecules (New York: Oxford Univ. Press)
Bernath, P. F., Black, J. H., & Brault, J. W. 1985, ApJ, 298, 375
Bonnell, J. T., & Bell, R. A. 1993, MNRAS, 264, 334
Boyer, R., Henoux, J. C., & Sotirovski, P. 1971, Sol. Phys., 19, 330
Branch, D. R. 1970, ApJ, 159, 39
Campbell, J. M., Klapstein, D., Dulick, M., Bernath, P. F., & Wallace, L. 1995, ApJS, 101, 237
Catanzaro, E. J., Murphy, T. J., Garner, E. L., & Shields, W. R. 1966, J. Res. NBS, 70A, 453
Choi, B.-G., Huss, G. R., Wasserburg, G. J., & Gallino, R. 1998, Science, 282, 1284
Cottrell, P. L. 1978, ApJ, 223, 544
Forsberg, P. 1991, Phys. Scr., 44, 446
King, A. S. 1916, ApJ, 43, 341
Kirby, K., Saxon, R. P., & Liu, B. 1979, ApJ, 231, 637
Kumar, C. K. 1969, BAAS, 1, 351
Lambert, D. L., Mallia, E. A., & Petford, A. D. 1971, MNRAS, 154, 26
Lambert, D. L., & McWilliam, A. 1986, ApJ, 304, 436
Lemoine, B., Demuynck, C., Destombes, J. L., & Davies, P. B. 1988, J. Chem. Phys., 89, 673
McWilliam, A., & Lambert, D. L. 1988, MNRAS, 230, 573
Mewaldt, R. A., & Stone, E. C. 1989, ApJ, 337, 959
Ram, R. S., Bernath, P. F., Dulick, M., & Wallace, L. 1999, ApJS, 122, 331
Saxon, R. P., Kirby, K., & Liu, B. 1978, J. Chem. Phys., 69, 5301
Selesnick, R. S., Cummings, A. C., Cummings, J. R., Leske, R. A., Mewaldt, R. A., & Stone, E. C. 1993, ApJ, 418, L48
Shetrone, M. D. 1996, AJ, 112, 2639
Sink, M. L., & Bandrauk, A. D. 1979, Canadian J. Phys., 57, 1178
Tomkin, J., & Lambert, D. L. 1976, ApJ, 208, 436
———. 1980, ApJ, 235, 925
Wallace, L., Livingston, W. C., Bernath, P. F., & Ram, R. S. 1998, An Atlas of the Sunspot Umbral Spectrum in the Red and Infrared from 8900 to 15050 cm^{-1} (6642 to 11230 Å) (Tech. Rep. 98-002; Tucson: NSO)
Zink, L. R., Jennings, D. A., Evenson, K. M., & Leopold, K. R. 1990, ApJ, 359, L65
Ziurys, L. M., Barclay, W. L., & Anderson, M. A. 1993, ApJ, 402, L21